National Oceanography Centre, Southampton

Research & Consultancy Report No. 84

On the shelf resonances of the Gulf of Carpentaria and the Arafura Sea

D J Webb

2011

National Oceanography Centre, Southampton
University of Southampton, Waterfront Campus
European Way
Southampton
Hants SO14 3ZH
UK

Author contact details
Tel: +44 (0)23 8059 6199
Email: djw@soton.ac.uk

DOCUMENT DATA SHEET

AUTHOR
WEBB, D J

PUBLICATION DATE 2011

TITLE
On the shelf resonances of the Gulf of Carpentaria and the Arafura Sea.

REFERENCE
Southampton, UK: National Oceanography Centre, Southampton, 16pp.
(National Oceanography Centre Southampton Research & Consultancy Report, No. 84)
(Unpublished manuscript)

ABSTRACT

A numerical model is used to investigate the resonances of the Gulf of Carpentaria and the Arafura Sea. The model is forced at the shelf edge, first with physically realistic real values of angular velocity. The response functions at points within the region show maxima and other behaviour which imply that resonances are involved but it is difficult to be more specific. The study is then extended to complex angular velocities and the results then show a clear pattern of gravity wave and Rossby wave like resonances. The properties of the resonances are investigated and used to reinterpret the responses at real values of angular velocity. It is found that in some regions the response is dominated by modes trapped between the shelf edge and the coast or between opposing coastlines. In other regions the resonances show cooperative behaviour, possibly indicating the importance of other physical processes.

KEYWORDS

ISSUING ORGANISATION
National Oceanography Centre, Southampton
University of Southampton, Waterfront Campus
European Way
Southampton SO14 3ZH
UK

On the Shelf Resonances of the Gulf of Carpentaria and the Arafura Sea

David J. Webb

National Oceanography Centre, Southampton SO14 3ZH, U.K.

Abstract.

A numerical model is used to investigate the resonances of the Gulf of Carpentaria and the Arafura Sea. The model is forced at the shelf edge, first with physically realistic real values of angular velocity. The response functions at points within the region show maxima and other behaviour which imply that resonances are involved but it is difficult to be more specific. The study is then extended to complex angular velocities and the results then show a clear pattern of gravity wave and Rossby wave like resonances. The properties of the resonances are investigated and used to reinterpret the responses at real values of angular velocity. It is found that in some regions the response is dominated by modes trapped between the shelf edge and the coast or between opposing coastlines. In other regions the resonances show cooperative behaviour, possibly indicating the importance of other physical processes.

1 Introduction

Recent studies by Arbic et al. (2009) and Green (2009) have again highlighted the question of the extent to which barotropic resonances affect the response of the ocean to external forcing. Because of their shape and bathymetry, one might expect to see resonances in both the deep ocean and the shelf seas. Both are of interest but the shelf resonances may be particularly important because of their potential impact on tidal power generation.

One can make a first estimate of the number of deep ocean resonances from studies such as that of Longuet-Higgins and Pond (1980). They calculated the resonant modes of a series of hemispherical oceans of uniform depth. Taking the ocean to have an average depth of 4000 m their results show that such an ocean would have eight resonant modes between one and two cycles per day (2π and 4π radians per day)[1] the density of modes increasing rapidly as the angular velocity increased.

Platzman (Platzman et al., 1981) investigated the resonances of a more realistic ocean and found 14 modes in the same band of frequencies. They also found a greater density of resonances at and beyond 4π radians per day.

As the tidal bands themselves have a width of approximately one radian per day one might expect to see the evidence of such modes in the tidal records. In contrast the analysis of tidal records, such as those discussed by Munk and Cartwright (1966), indicate that with the possible exception of the Coral sea region (Webb, 1973b), the response of the ocean is usually very smooth.

One possible explanation for this is that frictional effects are so strong that the resonances are damped out. This is consistent with a number of independent estimates of the residence of tidal energy in the ocean, that the decay time is of order 30 hours or less (Miller, 1966; Garrett and Munk, 1971; Webb, 1973a; Egbert and Ray, 2003). The equivalent decay time for the wave amplitude is twice this.

Bottom friction acting in the deep ocean is too small to produce such a rapid decay and the traditional view was that the energy was lost on continental shelves. Studies of satellite data (e.g. Egbert and Ray, 2001) have shown that a significant amount of tidal energy is lost to internal tides along mid-ocean ridges and other topographic features. However this is still less than the amount being lost on the shelves.

The loss of energy to the shelves was investigated by Webb (1976) who found that a tidal wave approaching a coastline from the deep ocean tended to be reflected back into the deep ocean with very little energy being lost on the continental

Correspondence to: D.J.Webb (djw@soton.ac.uk)

[1]To make the connection with the tides clearer this paper uses the 'practical' units of radians per day. In these units the diurnal tides lie near 2π radians per day and the semi-diurnal tides near 4π radians per day.

shelf. Exceptions were found to occur when the shelf is near resonance, i.e. when it is 1/4, 3/4 etc. wavelengths wide, but if the friction is too small or two large the tidal energy is till reflected back into the deep ocean. Thus a shelf will only have a significant effect in dissipating tidal energy if it has both the right dimensions and the right frictional properties.

Although this, and the more recent work of Arbic et al. (2009) on the coupling of the shelf sea modes to the deep ocean, gives us some confidence in the results, our understanding of the shelf sea resonances is still very limited. With this in mind the present paper reports some work on the response and resonances of the Gulf of Carpentaria and the Arafura Sea.

The area has been chosen for a number of reasons. First it enables use of a model which was previously validated in a study of the diurnal and semi-diurnal tides of the region. Thus, it should still give good results over the whole band of frequencies around one and two cycles per day.

Secondly it is a large continental shelf. It therefore might be expected to show many of the resonance features to be found elsewhere. Thirdly, related to point two, tidal observations indicate that in the north of Arafura Sea the region contains a classic quarter wavelength resonance. Tidal heights are smaller than those found in the classic resonance regions, such as the Bay of Fundy and the Bristol Channel, but it does provide an opportunity to learn more about such resonances.

Finally, and most importantly, the validated model is not limited to studies with real angular velocities. It also allows investigation of the complex angular velocity plane where each of the resonances produces a mathematical pole with an infinite response. This allows the properties of individual resonances to be investigated. Each resonance's contribution to the response of the real ocean can then be calculated and their interactions further studied.[2].

2 The Numerical Model

A numerical model is used to solve Laplace's tidal equations. In vector notation and with a linear friction term these are,

$$\begin{aligned} \partial \boldsymbol{u}/\partial t + \boldsymbol{f} \times \boldsymbol{u} + (\kappa/h)\boldsymbol{u} + g\nabla\zeta = g\nabla\zeta_e \,, \\ \partial\zeta/\partial t + \nabla\cdot(H\boldsymbol{u}) = 0 \,. \end{aligned} \tag{1}$$

$\boldsymbol{u}$ is the depth averaged horizontal velocity, t is time, ζ the sea level, ζ_e the height of the equilibrium tide (corrected for Earth tides), g the acceleration due to gravity, H the depth and '$\times$' indicates a vector product. The Coriolis vector $\boldsymbol{f}$ is defined by,

$$\boldsymbol{f} = 2\Omega\cos(\theta)\boldsymbol{n_z} \,, \tag{2}$$

[2]The present model was used in a similar way by Grignon (2005) to study the model of a simplified representation of the English Channel. It is hoped that a follow up study using a more realistic model of the region will be published soon.

where Ω is the Earth's rotation rate, θ the co-latitude, and $\boldsymbol{n_z}$ the unit vertical vector. The equations are obtained by integrating the full equations of motion in the vertical and neglecting the vertical acceleration, non-linear and self-attraction terms.

Eqn. 1 is linear, so the general solution for a given forcing can be written as a linear combination of solutions of the form,

$$\begin{pmatrix} \boldsymbol{u}(t) \\ \zeta(t) \end{pmatrix} = \Re[\begin{pmatrix} \boldsymbol{u} \\ \zeta \end{pmatrix} \exp(-i\omega t)] \,, \tag{3}$$

where ω is the angular velocity and $\Re$ represents the real part of the complex expression.

If we define P and $\boldsymbol{Q}$ as,

$$\begin{aligned} P &= g(iw - \kappa/h)/[(i\omega - \kappa/h)^2 + f^2] \,, \\ \boldsymbol{Q} &= \boldsymbol{f}/[(i\omega - \kappa/h)^2 + f^2] \,, \end{aligned} \tag{4}$$

then,

$$\boldsymbol{u} = (P + \boldsymbol{Q}\times)\nabla\zeta' \,, \tag{5}$$

where,

$$\zeta' = \zeta - \zeta_{eq} \,. \tag{6}$$

Substituting for $\boldsymbol{u}$ in 1,

$$\begin{aligned} HP\nabla^2\zeta' + [\nabla(HP) + \nabla\times(h\boldsymbol{Q})]\cdot\nabla\zeta_1' \\ -i\omega\zeta' = i\omega\ \zeta_{eq} \,. \end{aligned} \tag{7}$$

This is the equation that is solved numerically in the model. At coastlines the normal component of velocity is zero. If $\boldsymbol{n_c}$ is the unit vector normal to the coast, then using eqn. 4,

$$(P + \boldsymbol{Q}\times)\nabla\zeta'\cdot\boldsymbol{n_c} = 0 \,. \tag{8}$$

3 Numerical Solution

In the numerical model, the spherical co-ordinate form of eqn. 7 is replaced by a set of finite difference equations at the vertices of a rectangular grid, using a grid spacing of one eighth of a degree. The boundary condition, eqn. 8, is applied at points where the grid intersected coastlines, the finite difference equations taking into account both the angle between the coastline and the grid and the curvature of the coastline. Both coastline and depths were taken from Admiralty charts of the region.

In the original model, observed values of the tidal height were imposed on the open boundaries to the west of the Arafura Sea and on the eastern side of Torres Strait. For the more detailed study reported here the wave entering the region from the west is assumed to have unit amplitude and constant phase all along the western boundary. In the east, Torres Strait is now assumed to be blocked.

The use of a constant phase in the west is partly justified by the fact that the phase speed in the deep water along the

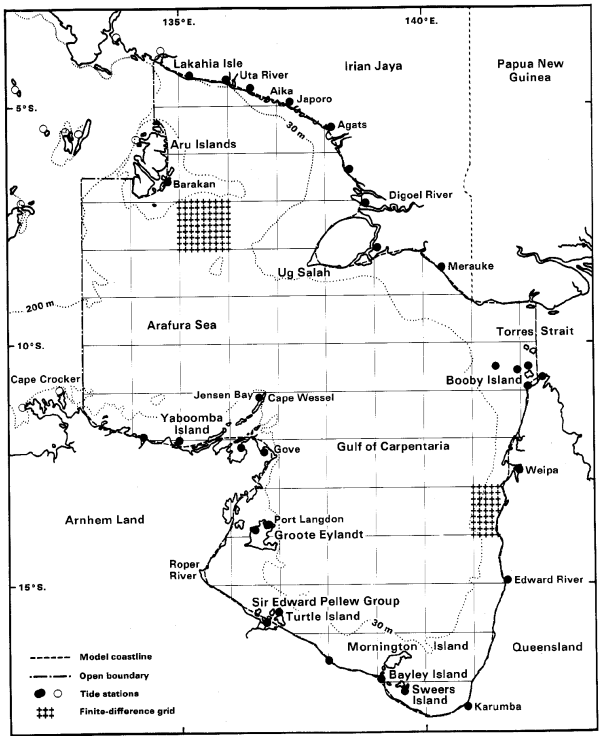

Fig. 1. Plan of the study area, showing the smoothed coastline used in the numerical model. ○ Tidal station used to determine the open boundary conditions. • Other tidal stations. Depth contours are shown as dotted lines. Islands whose coastlines are not represented in the model are replaced by water of depth 2.5 m.

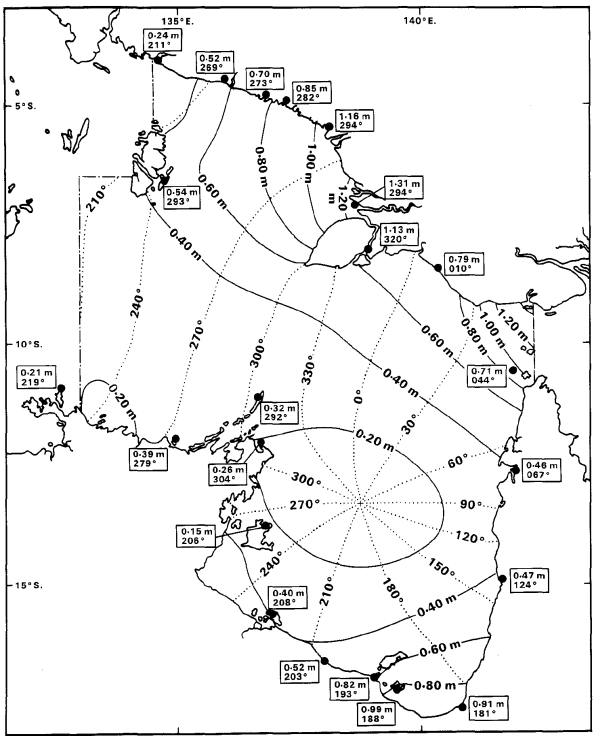

Fig. 2. Computed co-amplitude and co-phase lines for the K1 tide in the Gulf of Carpentaria and Arafura Sea. Observed amplitudes and phases, shown in the square boxes, are taken from Easton (1970) and from the Admiralty Tide Tables (Anon, 1971).

boundary is be much larger than on the shelf region being studied. Some difference in response is expected when the incoming wave does not have constant phase but the effect is likely to be small. In the east the amount of tidal energy entering through Torres Strait is small so the revised boundary condition, which simplifies the analysis, should have little effect on the large scale response of the region.

The coefficients resulting from the finite difference equations are loaded into a sparse matrix and the associated forcing terms into a corresponding vector. The full matrix equation is then solved using Gaussian elimination and back substitution, the numbering of the vertices being organised to minimise the size of the intermediate matrix. Further details of the model and solution are given in Webb (1981).

4 The Behaviour at Tidal Frequencies

Figures 2 and 3, reproduced from Webb (1981), show the results for the K1 and M2 tides. In the figures, the amplitude and phase lines are from the model and the boxed figures show the same quantities measured at tide gauges. There are discrepancies but they are relatively small.

The the K1 amplitude and phase lines indicate that, to a first approximation, the diurnal tide propagates along the northern boundary as a Kelvin wave and that it then circles clockwise around the Gulf of Carpentaria loosing energy on the way. However a simple decaying Kelvin wave would have an amplitude which declined monotonically with distance. Instead in the present case are four regions where the amplitude at the coast is a local maximum. Three of these, in corners of the Gulf may result from the Kelvin wave propagating around a nearly right-angled corner. The fourth, in the north-east of the Arafura Sea, near 138°, E 7°S, could be associated with a quarter wave resonance between the Digoel River[3] and the shelf edge.

In contrast, the semi-diurnal M2 tide shows no simple resemblance to a Kelvin wave. In the north of the Arafura Sea there appears to be a 3/4 wavelength wave, trapped between the shelf edge and the Digoel River. There are two additional maxima in the south of the Arafura sea and the North of the Gulf, which may be related, and a low amplitude east-west oscillation in the centre and south of the Gulf.

These results emphasise the fact that individual tidal constituents give little insight into the physical processes in-

[3]For locations see Fig. 1.

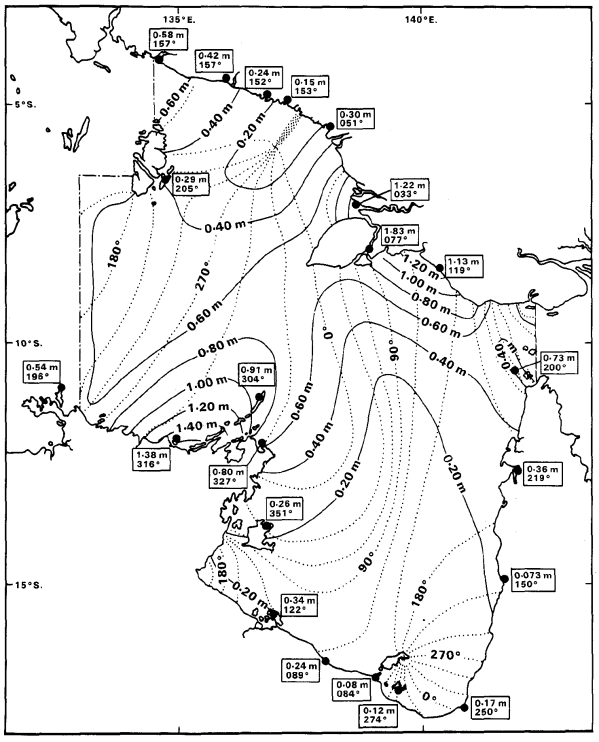

Fig. 3. Computed co-amplitude and co-phase lines for the M2 tide. Observed amplitudes and phases, shown in the square boxes, are taken from Easton (1970) and from the Admiralty Tide Tables (Anon, 1971).

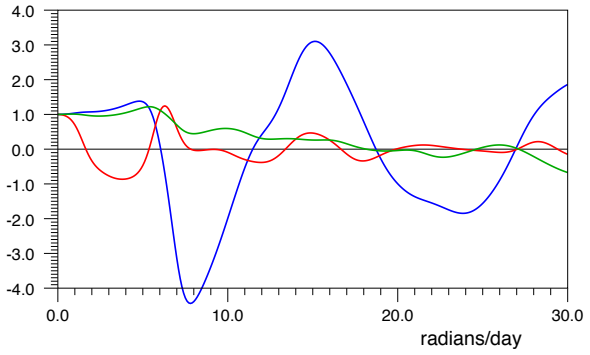

Fig. 4. Real component of the response functions between zero and 30 radians per day for Digoel River (blue) , Karumba (red) and Yaboomba Island (green).

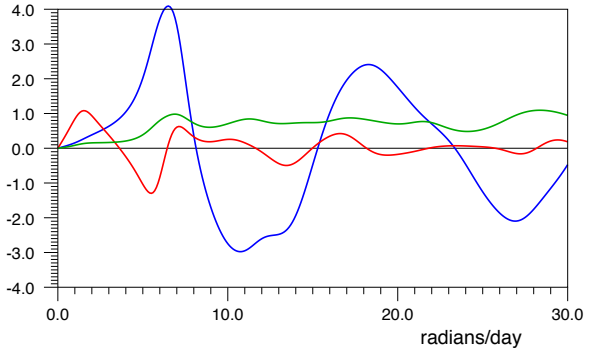

Fig. 5. Imaginary component of the response functions between zero and 30 radians per day. Colours as in figure 4.

volved. It is possible to repeat the analysis with other tidal constituents but the tidal bands are so narrow that little more can be learnt.

But in the present case the model is not limited to the tidal bands. It can be forced with a wide range of frequencies and so provide a wealth of additional information.

5 The Response Function

Using the new boundary conditions, the model was run at a series of frequencies between zero and 30 radians per day ($\sim$ 4.8 cycles per day). It is impractical to show co-tidal charts for all the frequencies calculated, so instead figs. 4, 5, 6 and 7 show the response R at three stations which have been selected to illustrate a range of behaviour. R is defined as,

$$R(x) = \zeta(x)/\zeta_b \,, \tag{9}$$

where $\zeta(x)$ is the (complex) tidal height at station x and ζ_b is the tidal height on the open boundary.

The first station is near Digoel River in the north of the Arafura Sea where both the diurnal and semi diurnal indicate the presence of standing waves. The second is near Karumba in the south-east of the Gulf of Carpentaria. Resonances don't appear to be a key feature of the region but there is a strong contrast between the diurnal and semi-diurnal tides. The final point is near Yaboomba Island on the southern boundary of the Arafura Sea. The diurnal tide appears as a simple progressive wave along the coast but the semi-diurnal tide appears to be affected by a resonance.

The results are presented here in three different ways. The first, in terms of the real and imaginary components of R, is the most fundamental and is closely related to the later exploration of the complex ω plane. The second, in terms of the amplitude and phase, is easier to relate to the physics and this is also true of the third, where the real and imaginary components are plotted against each other.

5.1 Real and Imaginary Components

Figures 4 and 5 show the real and imaginary components of the response function at each station. As the angular velocity tends to zero, all the real values tend to unity and the

imaginary values to zero, indicating that the tide everywhere follows that on the open boundary. As the angular velocity increases the functions diverge, the Digoel River showing the largest amplitude excursions. At Karumba the components have much smaller excursions especially at higher angular velocities but neighbouring maxima and minima are much closer than for the Digoel River.

The Yaboomba Island station shows is a slow decrease in the real component as angular velocity increases and there is a corresponding rise and plateauing of the imaginary component. Superimposed on this large scale behaviour there is a series of closely spaced maxima and minima similar to those at Karumba.

5.2 Amplitude and Phase

Figures 6 and 7, replot this data in the form of the amplitude and phase of the response. The amplitudes are all one at zero angular velocity but at higher values the behaviour is very different. Thus over most of the range the Digoel River amplitude is above two, it also shows very strong peaks near 7 and 14 radians per day and a weaker broader one near 27 radians per day.

The Karumba amplitude shows a small peak near 1.5 radians per day, a second one near 6 radians per day, but at higher angular velocities the amplitude is much reduced. There is a broad low peak around 13 radians per day and a further one around 30 radians per day but these are modulated by some structure which may be correlated with the Yaboomba Island response.

In contrast to both, the Yaboomba Island station remains close to unity over the whole range studied. There are a series of small maxima and minima at almost regular intervals, but these are better correlated with Karumba than with those of Digoel River.

The phase plots provide a different insight in that each of the three curves tends to have a constant slope over all of the frequency range considered. There are changes in slope, on the scale of the width of the peaks in the amplitude plot, but except for these feature the slope remains remarkably constant.

One possible way to understand this behaviour is to consider the response of a simple travelling wave,

$$\psi = A \exp(ikx - i\omega t) \; . \tag{10}$$

Assume that the wave speed is constant so that the k equals ω/c. Then if this wave is 'forced' so that it has amplitude one at the 'boundary' where x is zero, then at distance x, the response R will be simply,

$$R(\omega) = \exp(ikx) \; , \tag{11}$$

$$= \exp(i(x/c)\omega) \; . \tag{12}$$

In this case the gradient of the phase equals x/c, the time taken for the wave to propagate from the boundary.

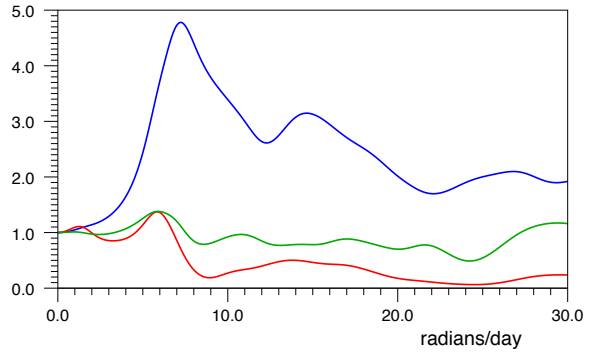

Fig. 6. Amplitude of the response functions between zero and 30 radians per day for Digoel River (blue) , Karumba (red) and Yaboomba Island (green).

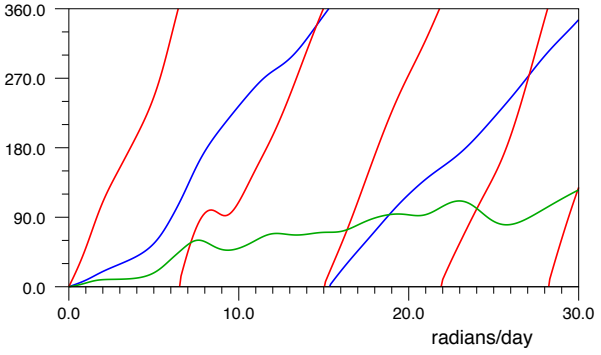

Fig. 7. Phase of the response functions between zero and 30 radians per day. Colours as in figure 6.

Applying this result to figure 7, it implies that on average incoming waves take one to two hours to reach the Yaboomba Island from the open boundary, about twelve hours to reach Digoel River and a day to reach Karumba. However the values differ somewhat from what might be expected from the phase lines of figs. 2 and 3. These indicate that the tidal wave takes longer, about four hours, to reach Yaboomba Island but slightly less, eighteen to twenty-four hours, to reach Karumba. Estimates for Digoel River are complicated by the standing wave affecting the semi-diurnal tide but the diurnal tide indicates about four hours whch is much less than the twelve hours estimated from fig. 7. Thus the simple idea of a progressive wave appears to be too simple and an alternative picture needs to be developed.

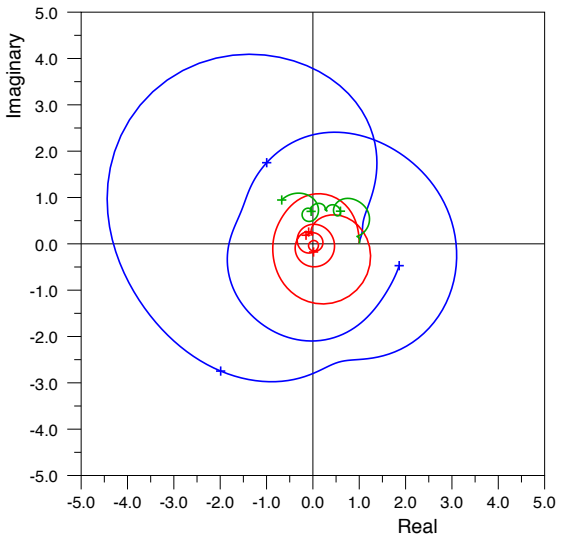

Fig. 8. Polar diagram showing the response functions between zero and 30 radians per day for Digoel River (blue), Karumba (red) and Yaboomba Island (green). The crosses are at intervals of 10 radians per day.

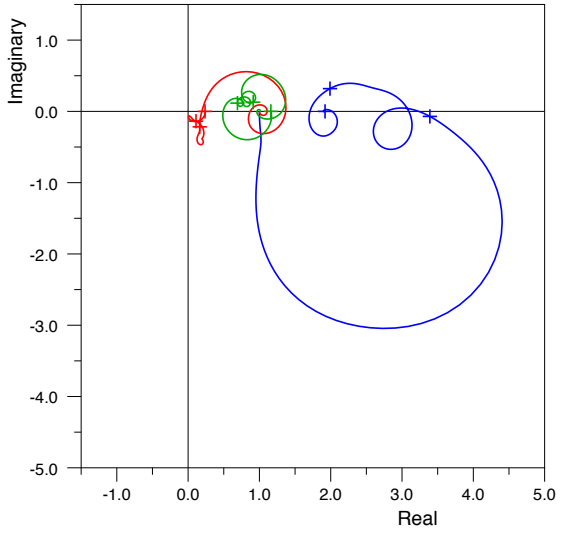

Fig. 9. Polar diagram showing the modified response functions (see text) between zero and 30 radians per day. Colours as in figure 8. The crosses are at intervals of 10 radians per day.

5.3 Resonance Circles

Webb (1973) discusses the form of the ocean's response to tidal forcing and shows that it has the form,

$$\psi(x,\omega) = \sum_j \psi_j(x) A_j/(\omega - \omega_j)\ , \qquad (13)$$

where x denotes position, ω is the angular velocity and ω_j is the angular velocity of the j'th resonance. $\psi_j(x)$ describes the spacial structure of the resonance and A_j depends on how the system is forced.

If the resonances are well separated, then near to each resonance the function at a fixed position has the form,

$$\psi(\omega) = R_j/(\omega - \omega_j) + B(\omega)\ . \qquad (14)$$

where $B(\omega)$ is a smooth background, the contribution of distant resonances.

Let ω_j have real and imaginary parts ω_{j0} and γ_j, where γ_j is usually negative. Then as ω moves along the real axis from minus to plus infinity, the resonance term increases from zero, to a to a value of iR_j/γ_j, when ω equals ω_{j0}, and returns to zero at plus infinity. It is straight forward to show (Webb, 2011) that as this happens the real and imaginary components move anti-clockwise around a circle that starts at the origin and passes through iR_j/γ_j at maximum distance from the origin.

Thus it may be possible to identify resonances in observations or model results, by plotting the real and imaginary components against each other and searching for clockwise circular features. However if $B(\omega)$ is rapidly varying this may be difficult. In particular circles are also produced by delays, such as those produced by the propagation of progressive waves discussed in the last section, but in such cases the circles are centred on the origin.[4]

To see how well the approach works for the present results, the real and imaginary components are plotted against each other in Fig. 8. All three curves start at the point $(1.0 + i0.0)$ and circle around the origin in an anti-clockwise direction. However although it is apparent that there are some underlying structures present in all three curve, only in the Yaboomba Island curve shows anti-clockwise circles and these are very small.

The main feature of the Karumba curve is that it circles the origin, initially at approximately unit distance, but finally it converges towards the origin. Thus as discussed before it appears to be primarily a progressive wave which is damped at higher angular velocities.

The Digoel River curve also circles the origin but at a distance which is much greater than one, so this cannot be a simple delay. However, in the absence of an alternative explanation, it is possible that the resonances which produce the peaks of Fig. 6, are overlapping or combining in such a way as to produce an effective delay.

In an attempt to remove the effect of the background, in fig.9, the data has been replotted which the phases are linearly corrected so that the total phase change over the whole band is zero. The transform will also distort the resonance circles, the distortion being proportional to the width of the

[4] In terms of the resonance picture, a progressive wave is the sum effect of many overlapping resonances.

resonance and the magnitude of the linear correction (greatest for Karumba) but the effect will be small if the resonances are narrow.

Now all three stations show a series of loops with a positive (anti-clockwise) curvature, as expected from resonances. At Karumba there are now some small kinks with negative curvature but these will have been produced by the transformation.

5.4 Analysis of Real Data

The results of this section show that analysis based on results with real values of the angular velocity is difficult. Plots of just the real or imaginary components as a function of angular velocity are not very useful. Peaks in the amplitude plots start to indicate the presence of resonances, three or four at Digoel River, six or seven at Yaboomba Island and a similar number at Karumba, but when additional confirmation is looked for in the phases the main feature appears to be a regular change in phases indicating, not resonances, but delays in the system. The final method, plotting the real and imaginary components against each other helps to confirm that resonances are being seen at Yaboomba Island but at the other two stations interpretation is again difficult.

It is possible that if all we had was data for real values of angular velocity, then more could be learnt by fitting the plotted data to a function similar to that of eqns. 13 or 14. However the present model can be run with complex values of angular velocity and, as is shown in the next section, this allows a more complete exploration of the complex plane.

6 The Complex ω plane

Figures 10 to 12 show the real component of the response at Digoel River, Karumba and Yaboomba Island plotted as a function of complex angular velocity. The data for the figures was created by running the model at intervals of 0.1 radians per day, in both the real and imaginary directions, between the origin and $(30-i10)$ radians per day. The data was then plotted in a view which looks beyond the real axis in the negative imaginary direction.

The values on the real axis are the same as in fig. 6 but the direction of increasing angular velocity is now towards the left. The values in the negative real direction (not plotted) are the mirror image of those in the positive direction. There are no poles in the positive imaginary direction.

The poles with negative imaginary values are the shelf resonances. Their positions correspond to the terms ω_j in eqn. 13 and are the same in all three figures. The apparent width of each peak is proportional to the magnitude of its residue, i.e. the term $\psi_j(x)A_j$ in the same equation. The differences between the residues in the three figures is thus a measure of the changing importance of each resonance in different parts of the Gulf.

The figures show that the resonances fall into two groups with a boundary near 4 radians per day. At lower angular velocities the resonances are tightly packed and in most cases the residues are small. They resonances also have a large range of decay rates, the imaginary component of angular velocity extending to minus ten and beyond.

Above 4 radians per day, the resonances are well separated and have much larger residues. At the lower (real) angular velocities, the imaginary components are one to two radians per day and these increase to three to four radians per day for the resonances near 30 radians per day.

This second group of resonances is also the one which appears to have the most influence on the diurnal and semi-diurnal tides. Table 1 contains a list of the resonances closest to the tidal bands plus resonances with low angular velocities which appear to have most effect on the low angular velocity response at Digoel River, Karumba and Yaboomba Island.

6.1 Gravity and Rossby Waves

Theoretical studies have shown that there are two main classes of long waves in the ocean, the gravity waves at high angular velocities, where energy is exchanged between potential and kinetic energy, and the Rossby waves at low angular velocities, where the exchange is primarily an exchange of kinetic energy between the two horizontal components of velocity.

Theory also shows that the boundary between the two regimes occurs at an angular velocity of f, the Coriolis parameter.

$$f = 2\Omega \sin(\theta) \,, \tag{15}$$

where θ is latitude and Ω is the angular velocity of the Earth. Waves with angular velocities near f are likely to show a mixture of both properties (Longuet-Higgins, 1968; Longuet-Higgins and Pond, 1980).

The Gulf of Carpentaria and the Arafura Sea span latitudes between 5°S and 18°S. This corresponds to values of the Coriolis parameter f, between 1.1 and 3.6 radians per day. Thus the change in properties seen near 4 radians per day can be identified as being due to the change from the Rossby wave to the gravity wave parts of the spectrum.

If eqn. 1 is used to study the decay of a steady current, it is easy to show that the decay rate is proportional to κ/h, where κ is the friction parameter and h the depth. Webb (2011) investigated gravity wave resonances in a simple 1-D model with a constant depth continental shelf and showed that the resonance decay rates, the imaginary parts of the complex angular velocity, were given by the same equation.

In the model, κ has the value $0.1\ \mathrm{cms}^{-2}$ and the depths range from over $100\ \mathrm{m}$ in parts of the Arafura sea and $70\ \mathrm{m}$ in the centre of the Gulf of Carpentaria to $20\ \mathrm{m}$ and less near to the coastline. Using the above equation, a depth of $100\ \mathrm{m}$ gives a decay rate of $0.86\ \mathrm{day}^{-1}$ and this increases to $1.73\ \mathrm{day}^{-1}$ for a depth of $50\ \mathrm{m}$, $3.46\ \mathrm{day}^{-1}$ for $25\ \mathrm{m}$ and 8.64

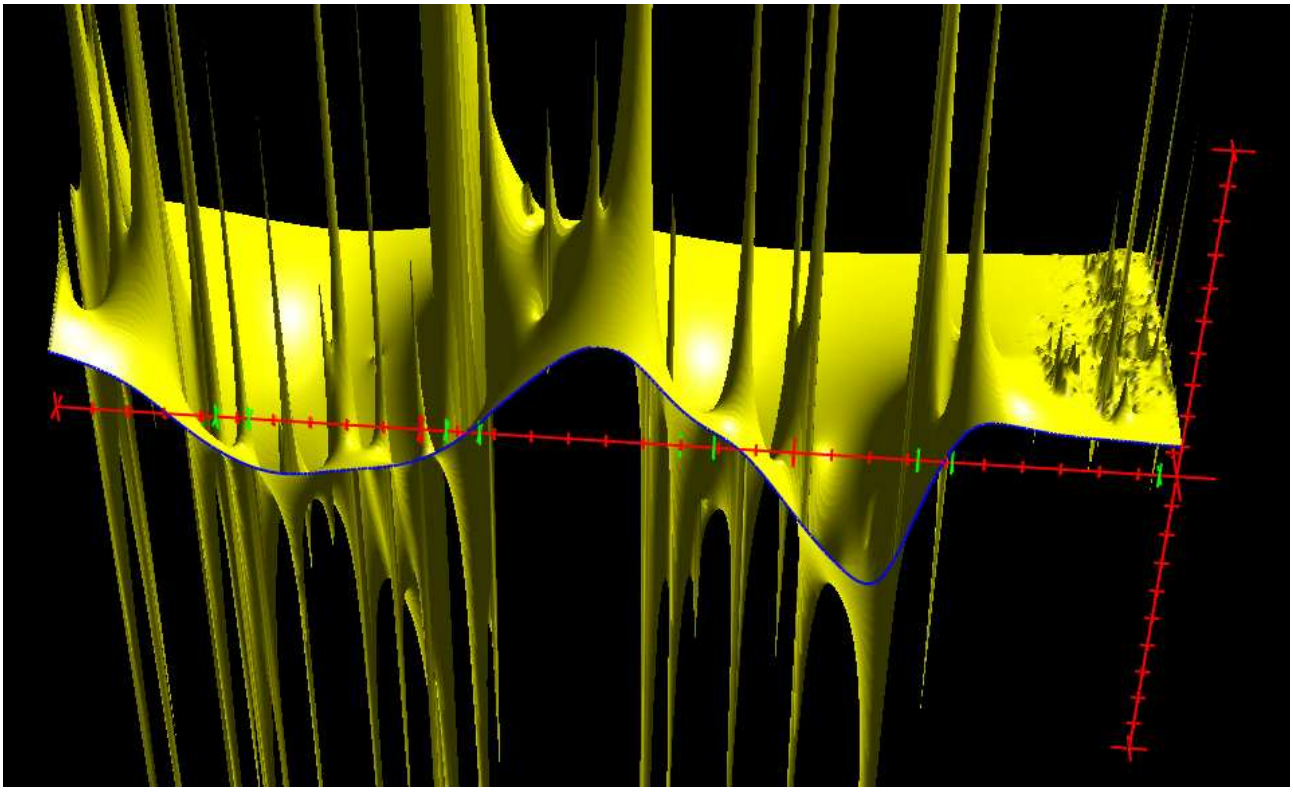

Fig. 10. Real part of the response function at Digoel River plotted as a function of complex angular velocity between (0 + i0) and (30 - i10 radians per day. Axes in red with ticks every unit interval. The origin is on the right with the real axis extending to the left and the negative imaginary axis extending backwards. The green ticks indicate the long-period, diurnal, semi-diurnal and higher tidal bands. The blue line is the response at real angular velocities as plotted in figure 4 but with the direction of the real axis reversed.

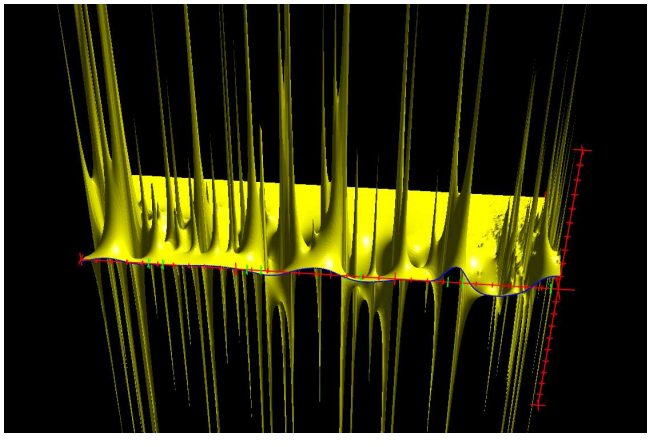

Fig. 11. Real part of the response function at Karumba. Details as in figure 10.

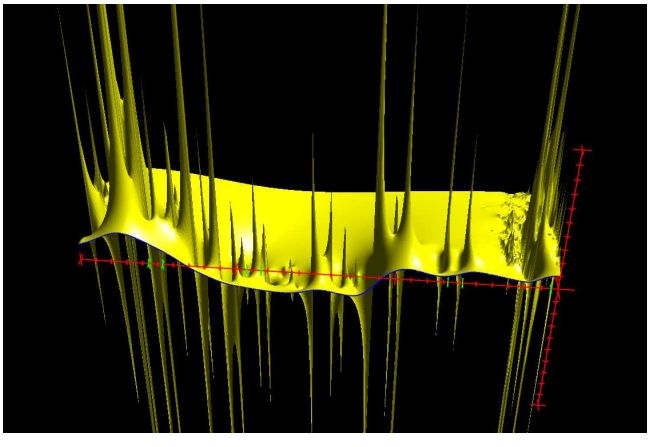

Fig. 12. Real part of the response function at Yaboomba Island. Details as in figure 10..

day^{-1} for $10\,\mathrm{m}$. The gravity wave values of Table 1, are thus consistent with mean depths of between 25 and 50 m, values which are not unreasonable.

Rossby waves on a shelf of constant depth are also expected to have decay rates of κ/h. Thus the Rossby wave resonances of the current model with decay rates of $10\,\mathrm{day}^{-1}$

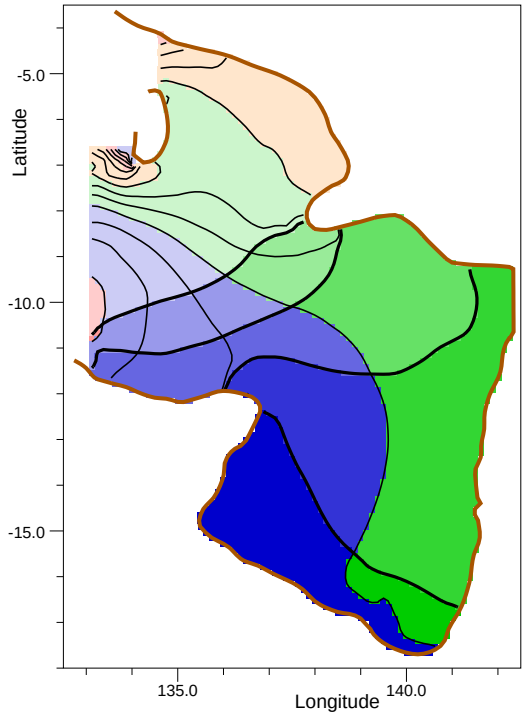

Fig. 13. Amplitude and phase contours for resonance aa. The phase contours (light) are at intervals of 30 degrees, colour coded with red in the quadrant -180°to -90°, brown -90°to 0°, green 0°to 90°and blue 90°to 180°. Amplitude is is in the range 0 to 1, with contours (heavy) at intervals of 0.2 and darker colours indicating greater amplitude. Amplitude is zero on the open (western) boundary and at the centre of amphidromes, and has the value 1 at points with maximum amplitude.

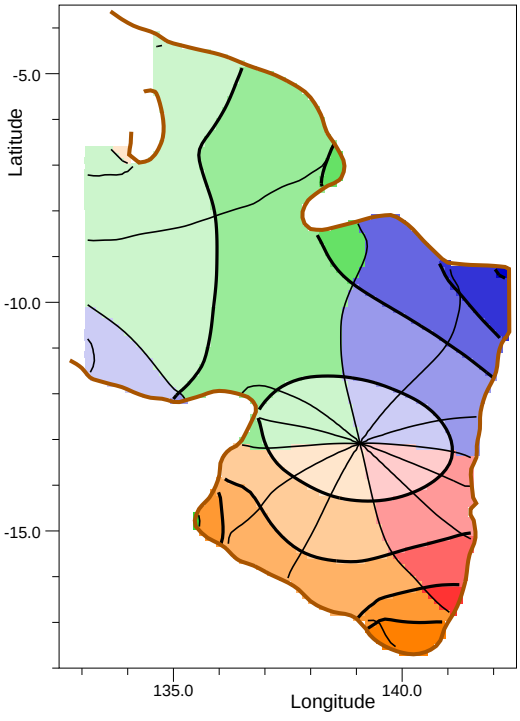

Fig. 14. Amplitude and phase contours for resonance A. Contours as in figure 13.

must be in regions of the shelf where the depth is near $10\ \mathrm{m}$. There should also be gravity wave resonances with similar decay rates but these presumably occur at much higher angular velocities than the range explored here.

7 The Resonances

The angular velocity of the resonances can be found by fitting equation 14 to the calculated response function in the neighbourhood of each resonance. Use was made of the four nearest values and these were fitted using a linear background,

$$\psi(\omega) = R_j/(\omega - \omega_j) + A + B\,\omega\,. \qquad (16)$$

As discussed in Appendix I, this can be converted into a linear matrix equation and so solved for the unknowns including the resonance frequency ω_j. The results for the main resonances using the data from Digoel River are given in table 1. The results obtained from using any of the other stations are essentially the same.

Once the angular velocity of a resonance is known, the spatial structure can be calculated in a similar manner. This time solutions to the model equations were obtained for each the four angular velocities $\omega \pm \delta\omega$ and $\omega \pm \imath\delta\omega$, where $\delta\omega$ equalled 0.1 radian/day. Again, further details of the method used, which makes use of the properties of Vandermonde matrices, are given in Appendix 1.

Table 1. Real and Imaginary components of angular velocity (in radians per day) for some of the key resonances plus the names used to refer to them in the text.

	Angular velocity			Angular velocity	
	Real	Imag.		Real	Imag.
aa	1.4561	-1.1419	K	15.3736	-1.6588
bb	3.1370	-1.6373	L	16.7251	-2.0066
A	5.8397	-1.1277	M	16.9845	-3.5121
B	7.0215	-1.3056	N	17,4437	-3.2135
C	7.8389	-2.0418	O	18.4964	-2.6164
D	9.5938	-2.0780	P	19.1721	-2.7670
E	10.2025	-2.6180	Q	20.0978	-3.4472
F	11.4272	-1.7270	R	20.4820	-1.8994
G	12.6226	-2.4655	S	20.6322	-3.3178
H	13.3884	-2.2500	T	21.4129	-1.9414
I	14.1413	-2.2405	U	22,5463	-2.6505
J	14.8486	-2.5489			

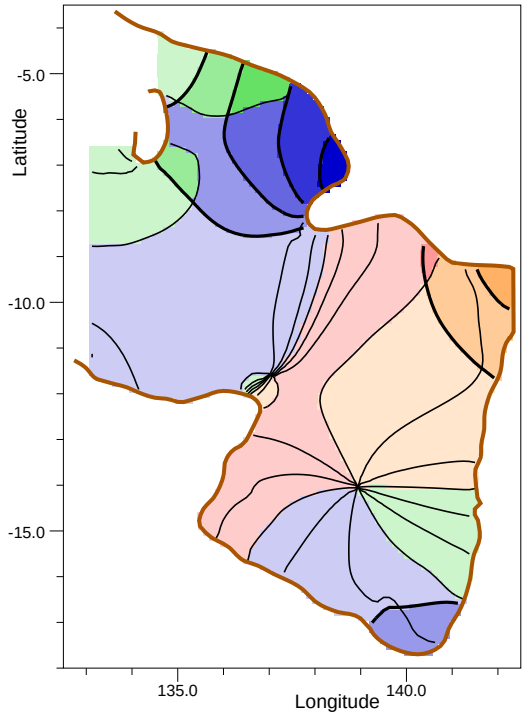

Fig. 15. Amplitude and phase contours for resonance B. Contours as in figure 13.

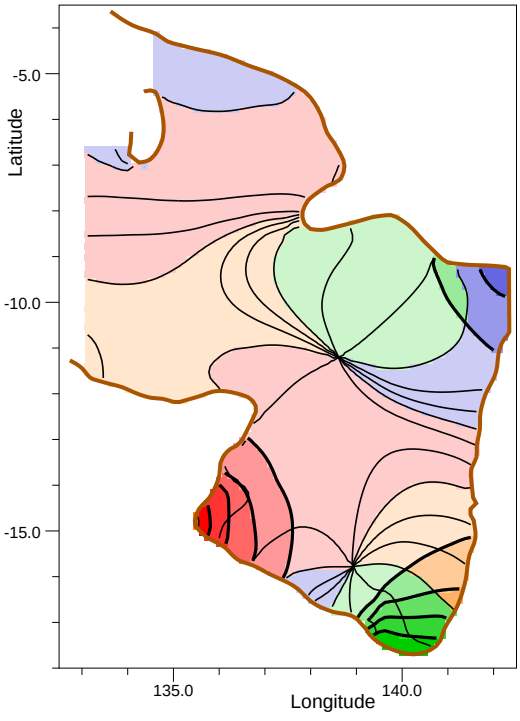

Fig. 16. Amplitude and phase contours for resonance C. Contours as in figure 13.

7.1 Resonance Waveforms

Figures 13 to 21 show the amplitude and phase of some of the main resonances affecting the diurnal and semi-diurnal tides in the region. Mode aa is included because it is the fundamental quarter-wavelength mode, having a maximum at the southern limit of the Gulf of Carpentaria. However it is not a classical quarter wavelength resonance because its angular velocity is less than the Coriolis parameter everywhere except near the northern coastline of the Arafura Sea. As a result its properties are those of a Rossby wave with only a small fraction of its energy in the form of potential energy. Thus even at low angular velocities it has only a limited effect on tidal height [5].

The remaining resonances illustrated are all primarily gravity wave modes and as such each of them might dominate the response with a suitable pattern of forcing. However in the present case the forcing is limited to the shelf edge and this appears to limit the importance of individual resonances and they way they interact.

At low angular velocities, resonances A, B and C are well separated in angular velocity from other resonances and are relatively weakly damped. As a result one might expect them to dominate the response in the diurnal tide band and, as discussed later, this is the case.

Figures 14 and 16 show that resonances 'A' and 'C' are both primarily progressive waves trapped within the Gulf of Carpentaria. Their angular velocities appear to be determined by 'A' fitting a single wavelength around a single amphidrome and 'C', two wavelengths around a double amphidrome.

In contrast resonance 'B' (fig: 15) is primarily a quarter wavelength wave trapped between the shelf edge and the Digoel River. Some energy does propagate into and circulate around the Gulf of Carpentaria but it appears to be the distance between the shelf edge and the Digoel River which determines the angular velocity of this mode. The angular velocities of resonances 'B' and 'C' are very close, so it is possible that this results in some mixing of the solutions.

At higher angular velocities the structure of the resonances becomes more complex and it is more difficult to relate them to physical features. One exception is resonance 'F' which appears to be primarily a standing wave trapped between the northern boundary of the Gulf of Carpentaria and the southern boundary of the Arafura Sea. Another is resonance 'I' which is a three-quarters wave trapped between Digoel River and the shelf break. Note that this time there is very little coupling to the Gulf of Carpentaria.

The remaining resonances have a more irregular structure.

[5] Grignon (2005) showed that the fundamental mode of the English Channel has similar properties

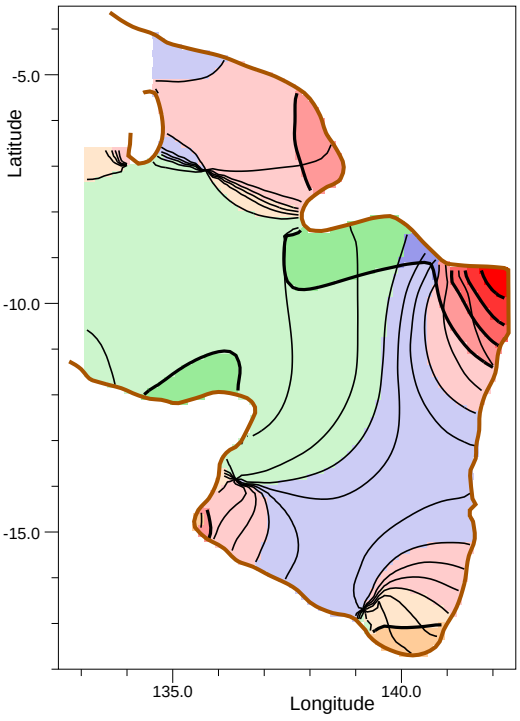

Fig. 17. Amplitude and phase contours for resonance D. Contours as in figure 13.

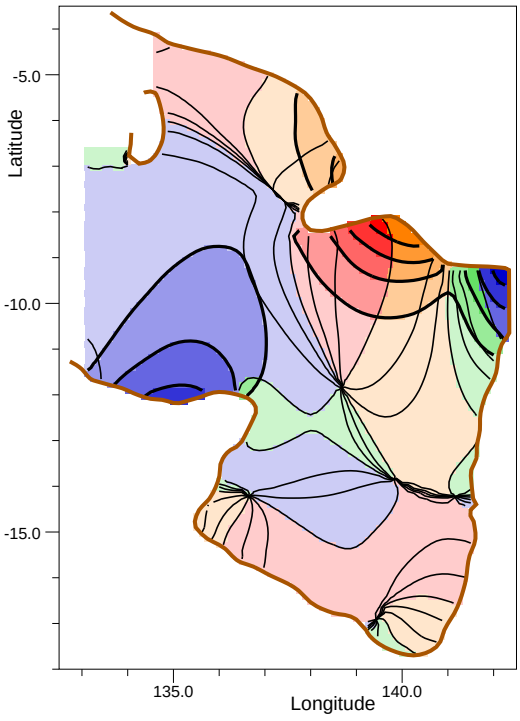

Fig. 19. Amplitude and phase contours for resonance F. Contours as in figure 13.

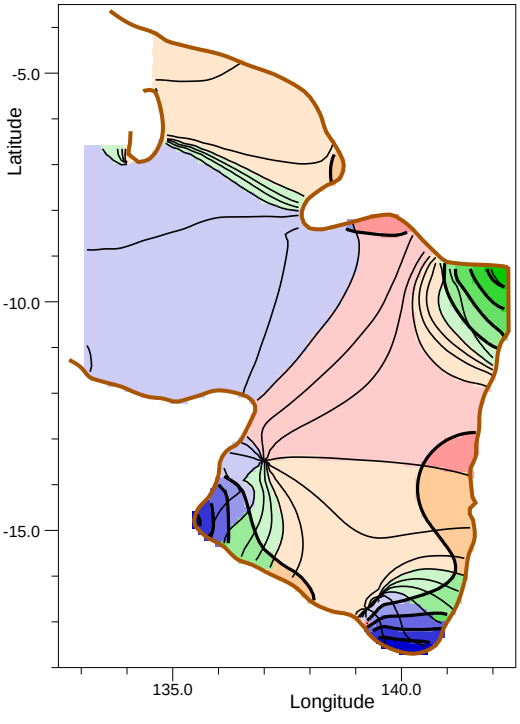

Fig. 18. Amplitude and phase contours for resonance E. Contours as in figure 13.

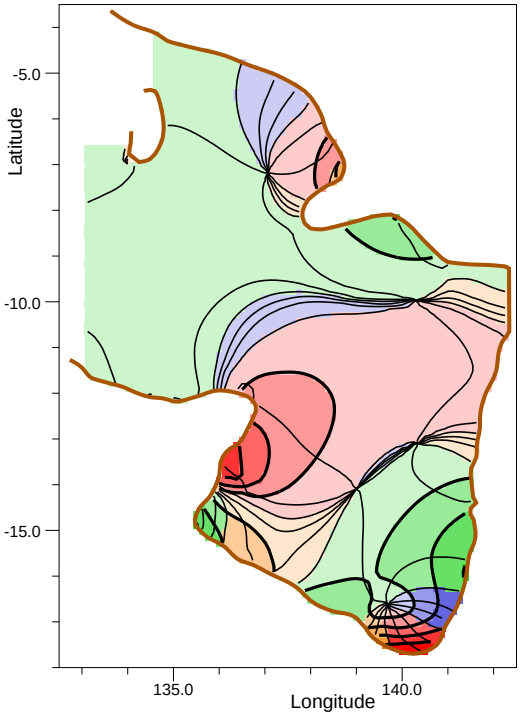

Fig. 20. Amplitude and phase contours for resonance H. Contours as in figure 13.

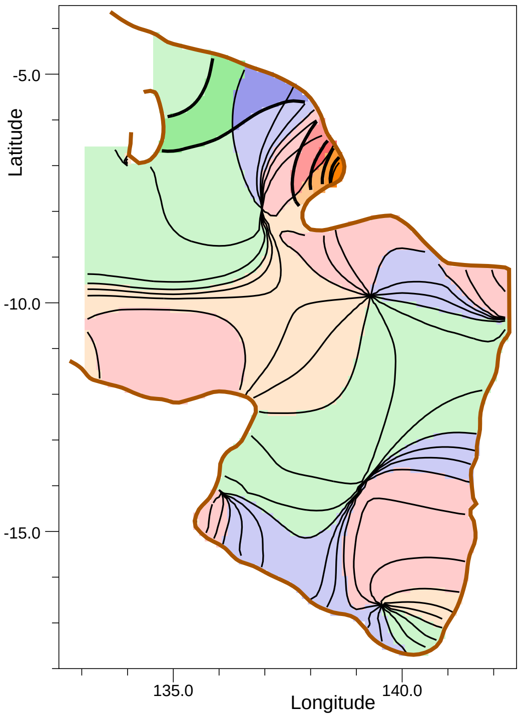

Fig. 21. Amplitude and phase contours for resonance I. Contours as in figure 13.

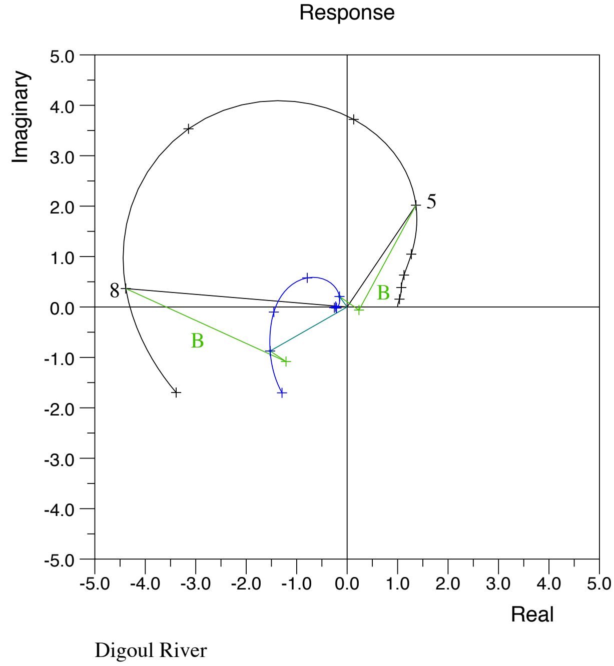

Fig. 22. Polar plot of response function (black) at Digoel River, for the range 0 to 9 radians per day. The black crosses are at intervals of one radian per day. The contribution of the resonance B, and its complex conjugate, is plotted in green at 5 and 8 radians per day, the conjugate contribution being the smaller. The residual after subtracting the contribution of resonance B is plotted in blue, also for the range 0 to 9 radians per day.

Many of them, like resonance E, have maxima in corners of the Gulf of Carpentaria but the increasingly complex pattern of phases indicates that their main role is to provide the complete set of functions required to describe all possible wave patterns.

8 Resonances and Real Angular Velocities

The polar plots, discussed earlier, showed that at real values of the angular velocity the presence of resonances could be indicated by the presence of tight loops in the response function. Here use is made of this property to identify the resonances responsible for the key features of the response function in the diurnal and semi-diurnal bands. Over such a band, it should be possible to expand the response function $R(x,\omega)$ at site x as,

$$R(x,\omega) = \sum_j R_j(x)/(\omega - \omega_j) + c.c. + B(x,\omega)\,, \qquad (17)$$

where the sum j is over a limited number of key resonances and $B(x,\omega)$ is a smooth background. $R_j(x)$ and w_j are the values calculated in the previous section.

The choice of key resonances is to a certain extent subjective. In the examples given here it was done by finding a set of resonances which, over the band of real angular velocities considered, both reproduced the main features of the response function and left a residual which was small and smooth.

The results are illustrated using the polar form of the response function figures. The full response function and the background term are plotted for the whole band and the individual contributions from the selected resonances and their complex conjugates are plotted at two points within each band. Because of the difference in angular velocity, the complex conjugate contributions tend to be small except zero angular velocity.

Two bands of angular velocities are considered. The first extends from zero to nine radians per day. This covers the diurnal tides and also shows the behaviour at very low values of angular velocity. The second band extends from ten to fifteen radians per day and covers the semi-diurnal tides.

8.1 The Diurnal Band

The result for Digoel River for the band 0 to 9 radians per day is shown in fig. 22. The large amplitude loop in the response function can all be explained by the changing amplitude and phase of the contribution of resonance B, a quarter wavelength resonance. The background term is seen to grow with angular velocity, reaching an amplitude of two by 8 radians per day but it still remains much smaller than the single resonance contribution.

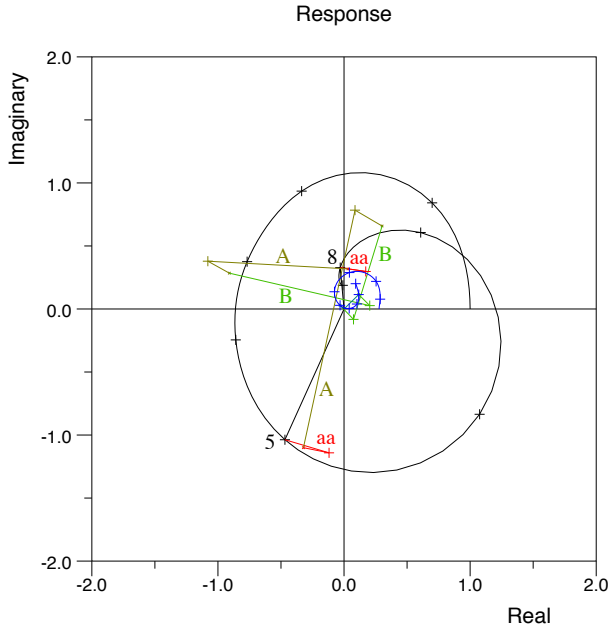

Karumba

Fig. 23. Polar plot of response function (black) at Karumba, for the range 0 to 9 radians per day. The black crosses are at intervals of one radian per day. The contribution of the resonances aa (red), A (yellow) and B (green), and their complex conjugates, are plotted at 5 and 8 radians per day, the conjugate contribution being the smaller. The residual after subtracting the contribution of these resonances is plotted in blue, also for the range 0 to 9 radians per day.

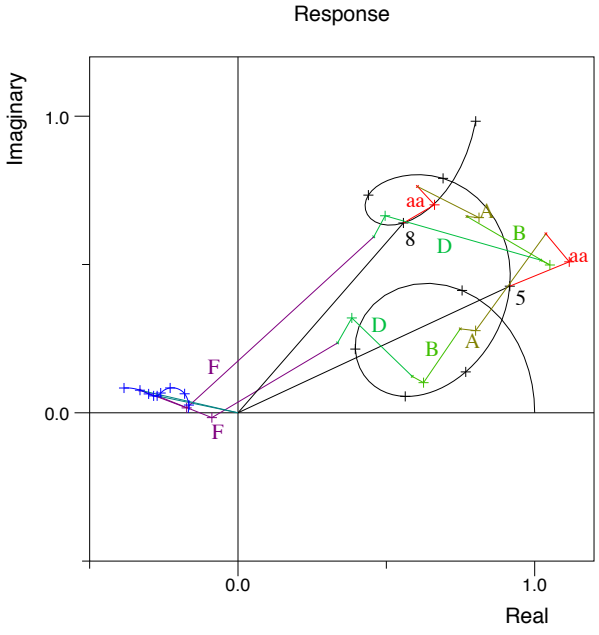

Yarumba Island

Fig. 24. Polar plot of response function (black) at Yaboomba River, for the range 0 to 9 radians per day. The black crosses are at intervals of one radian per day. The contributions of the resonances aa (red), A (yellow), B (green), C (light blue), and D (dark blue), and their complex conjugates, are plotted at 5 and 8 radians per day, the conjugate contribution being the smaller. The residual after subtracting the contribution of these resonances is plotted in blue, also for the range 0 to 9 radians per day.

The corresponding result for Karumba is shown in fig. 23. At low angular velocities it was found necessary to include resonance 'aa' in order to reduce the background at near zero angular velocity. For the 5 to 8 radians per day region, which includes the diurnal tides, it was found necessary to include both 'A' and 'B' resonances. These both have large amplitudes and phase changes of around 90°.

More importantly they have approximately opposite phase. Near 5 radians per day the contribution from resonance 'A' is large and 'B' only reduces it slightly. However by 8 radians per day they are effectively cancelling each other out and this results in a much lower amplitude response function. Figures 2 and 3 show that the semi-diurnal tides at Karumba are low compared with the diurnal tides and this might have been thought to be a result of an increase in the effect of friction at higher angular velocities. However in the present case both model have similar decay times and so the reduction in amplitude is purely an effect of interference between the two modes.

A further complication is found is found in the results for Yaboomba Island (fig. 24). The first loop is found to be primarily the effect of the Rossby wave resonance 'aa'. Resonances 'A' and 'B' are also significant. They again show an approximately 90° phase change between 5 and 8 radians per day, but here they are acting in phase and as a result produce the increase in amplitude near 5 radians per day. Two more resonances 'D' and 'F' are also significant and as the angular velocity increases they grow even larger. From figs. 17 and 19 they both involve a standing wave between the southern boundary of the Arafura Sea and the north of the Gulf of Carpentaria. Together they both contribute towards completing the second loop of the response function and the further increase in its amplitude past 8 radians per day.

8.2 The Semi-diurnal Band

Figure 25 shows the response function at Digoel River in a range including the semi-diurnal tides. Resonance 'B' is still significant but it is declining in importance and a large number of other resonances are now involved. These include 'D', 'F', 'H' and 'P', all of which show noticeable phase changes between 11 and 14 radians per day, but the largest contribution is now from 'I', the three-quarter wave resonance trapped between the Digoel River and the shelf edge.

At Karumba, fig. 26, all of the resonances in the range 'D' to 'K' now make significant contributions. The largest amplitude term is that of 'H', a rather complex resonance confined to the Gulf, but its effect is to a large extent cancelled out by other resonances. However its increased amplitude does seem to be responsible for the second partial loop seen around 14 radians per day.

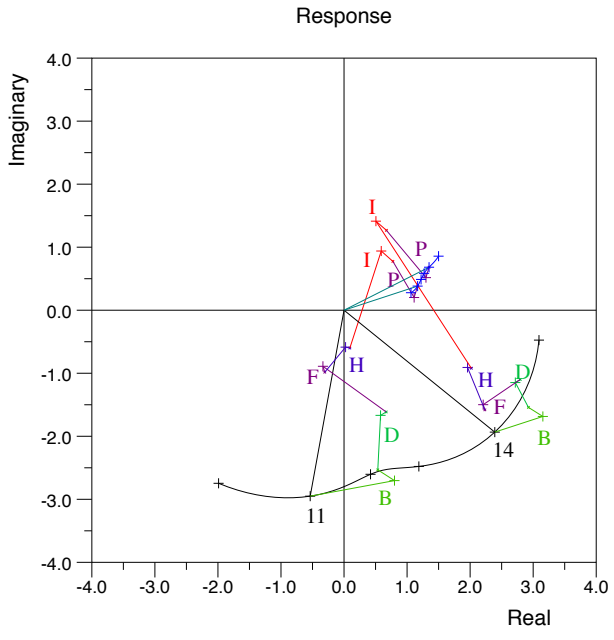

Digoul River

Fig. 25. Polar plot of response function (black) at Digoel River, for the range 10 to 15 radians per day. The black crosses are at intervals of one radian per day. The contribution of the resonances B, D, H, I, and P, and their complex conjugates, are plotted at 11 and 14 radians per day, the conjugate contribution being the smaller. The residual after subtracting the contribution of these resonances is plotted in blue, also for the range 10 to 15 radians per day.

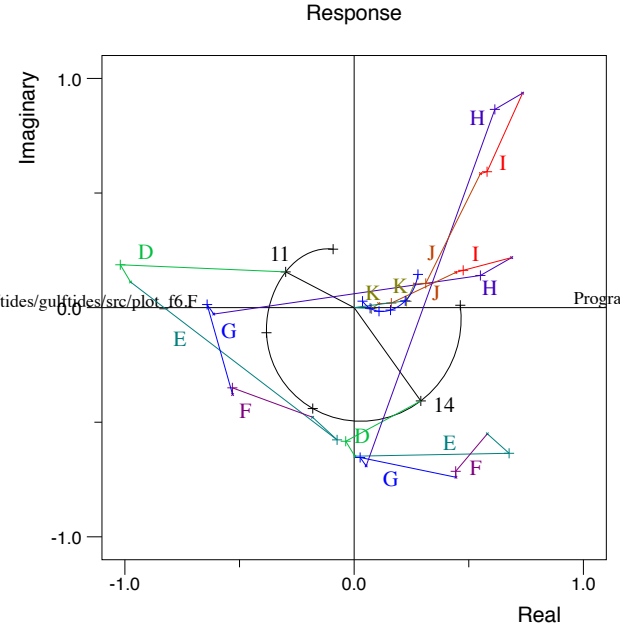

Karumba

Fig. 26. Polar plot of response function (black) at Karumba, for the range 10 to 15 radians per day. The black crosses are at intervals of one radian per day. The contribution of the resonances D to K, and their complex conjugates, are plotted at 11 and 14 radians per day, the conjugate contribution being the smaller. The residual after subtracting the contribution of these resonances is plotted in blue, also for the range 10 to 15 radians per day.

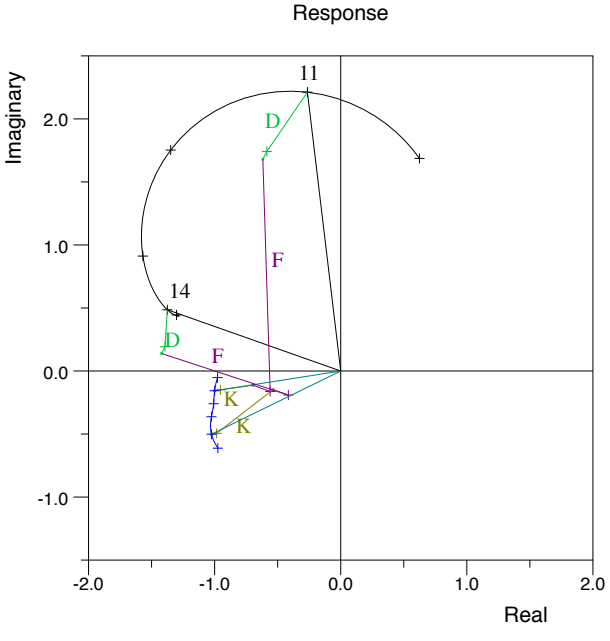

Yarumba Island

Fig. 27. Polar plot of response function (black) at Yaboomba Island, for the range 10 to 15 radians per day. The black crosses are at intervals of one radian per day. The contribution of the resonances D, F and K, and their complex conjugates, are plotted at 11 and 14 radians per day, the conjugate contribution being the smaller. The residual after subtracting the contribution of these resonances is plotted in blue, also for the range 10 to 15 radians per day.

Program: occam/tides/gulftides/src/plot_f6.F

Program: occam/tides/gulftides/src/plot_f6.F

Cancellation is also seen within the group of resonances 'E', 'F', and 'G'. Resonances 'A'. 'B' and 'C' (which for clarity are not plotted) cancel each other in a similar manner.

In contrast to Digoel River and Karumba, the number of significant resonances contributing to the response function at Yaboomba River has dropped (see fig. 27). 'F' is the largest resonance, responsible for the main loop, and only two more, 'D' and 'F', are required to smooth the background. The result confirms that the unusual standing wave between the southern boundary of the Arafura Sea and the northern boundary of the Gulf of Carpentaria is a key feature of the region.

9 Discussion

The primary aim of the work reported has been to learn a little of the properties of resonances associated with a realistic section of continental shelf. The Gulf of Carpentaria and Arafura Sea region was chosen because a validated model of the region was available and because there were indications that resonances were present, especially in the region between the Digoel River and the shelf edge. The model also had the advantage that it could be used to investigate both real and complex values of angular velocity

The model was forced near the shelf edge and it was first used to investigate the response of the region as the angular velocity varied over the tidal bands. This stage only used real angular velocities and interpretation of the results was difficult. The amplitude of the response function showed peaks but these were not simple ones that one may expect from a single resonance. The phase diagrams indicated that the wave generated by the forcing may be largely simple progressive waves which are only slightly modified by some other process. However the polar diagrams showed a number of tight loops with positive curvature. Theory predicts that isolated resonances will generate such looks

The theory of linear systems also shows that the response functions can be continued as analytic function into the complex angular velocity plane. The resonances then show up as poles in the analytic functions, the real components of the poles position giving the real angular velocity of the resonance and the imaginary component giving its decay rate.

The model was used to investigate the complex plane. It showed the existence of a rich pattern of resonances with a band of large poles extending from six radians per day to to higher angular velocities. These were identified as gravity wave like resonances of the region. There was also a field of smaller poles with small real angular velocities but with a large range of imaginary angular velocities. These were identified as the Rossby wave like modes.

An investigation of the modes showed that some of the gravity like modes, especially those with low (real) angular velocities, could be identified as fundamental 1/4 or 3/4 wavelength modes fitting between the shelf edge and the coast or modes associated with reflection between opposing boundaries. Others were much more complex, whose main role may be to contribute to the complete set of modes needed to describe all possible waveforms within the system.

The Rossby wave like modes were not investigated in the same way but one of them was found to be a 1/4 wavelength wave trapped between the shelf edge and the southern boundary of the Gulf of Carpentaria. If there was no Coriolis terms this would have been the fundamental quarter wavelength mode of the system and have a significant effect. However here it is at such a low angular velocity that it is primarily a Rossby wave and so has less effect on wave height.

Finally the results using real values of angular velocity were reinterpreted making use of the know angular velocities and waveforms of the resonances. There are only a few resonances close to the diurnal band and these were found to dominate the response within the band. There are more resonances close to the semi-diurnal band and the behaviour there was found to be more complicated.

However the results show that in both bands there are regions where the response is strongly influenced by the fundamental resonances that are trapped between the shelf edge and the coast or between two opposing coastlines. Elsewhere the resonances often appear to produce cooperative effects, a group of resonances forming a single 'resonant like' loop, cancelling each others contributions or producing an approximation to a simple progressive wave.

The apparent cooperation may simply reflect the fact that in such regions the separation, in complex angular velocity, between such resonances is less than their distance from the real axis. Alternatively it may be an indication that, where it occurs, the physical process involved is one for which a simple resonance interpretation is the wrong one. This should occur, for example, in the case of a simple progressive wave. The resonance picture may also be inappropriate for a slowly narrowing channel many wavelengths long, for which a W.K.B. approximation may be more relevant. However the fact that the 1/4, 3/4 and other simple resonances stand out so clearly implies that such resonances are still likely to be important in other regions of the world's ocean.

One important consideration that has not been discussed so far is the fact that the continental shelf modelled here is not connected to a realistic deep ocean. Webb (2011) investigates this problem for the simple case of a one-dimensional shelf coupled to a similar deep ocean. The results indicate that the main change is that the resonances loose some energy into the deep ocean and so they have a shorter decay time (i.e. a more negative imaginary component of angular velocity). In terms of the present results, this would tend to broaden the resonances - possibly reducing their individual effects and increasing the cooperative behaviour.

A second concern is how the modes are coupled to the deep ocean resonances. As discussed by Arbic et al. (2009) one might expect the coupling to be strong only for cases where the deep ocean and shelf resonances have similar angular velocities. But given the apparent importance of resonant shelves in loosing tidal energy, it may also be that strong coupling only occurs where the shelf resonance can have a significant damping effect on the deep ocean mode. This needs further investigation.

It is hoped that the present papers novel approach to the response of the ocean in the tidal bands is of use. Its limitation to a single continental shelf is unfortunate but it is hoped that its extension to a more realistic global ocean may eventually be possible.

Appendix 1. Resonance and Background

The problem is to fit a series of response function values $R(\omega_i)$ for different values of ω_i by a single resonance and a linear background,

$$R(\omega_i) = R_j/(\omega_i - \omega_j) + P + Q\,\omega_i\,. \tag{18}$$

P and Q are complex constants, ω_j is the complex angular velocity of the resonance and R_j its residue. This is a specific form of the more general problem if fitting a set of values y_i and x_i to an equation of the form,

$$y = A/(x - B) + \sum_{n=0}^{N} C_n x^n\,. \tag{19}$$

Multiplying by $(x - B)$,

$$y(x-B) = A + \sum_{n=0}^{N} \left(C_n x^{n+1} - C_n B x^n\right) , \tag{20}$$

$$yx = A + By - C_0 B + \sum_{n=1}^{N} (C_{n-1} - C_n B)x^n + C_N x^{N+1} ,$$

$$yx = (A - C_0 B) + By + \sum_{n=1}^{N} (C_{n-1} - C_n B)x^n + C_N x^{N+1} .$$

This can be written in the form,

$$yx = D_0 y + \sum_{n=1}^{N+2} D_n x^{n-1} . \tag{21}$$

This like eqn. 19 has N+3 unknowns. If a similar number of pairs of values x and y are available it gives a matrix equation which can be solved using standard methods for the unknowns $\boldsymbol{D}$. Then,

$$\begin{aligned} B &= D_0 , \\ C_N &= D_{N+2} , \\ C_{n-1} &= D_{n+1} + C_n B \; for \; n = 1...N , \\ A &= D_1 + C_0 B . \end{aligned} \tag{22}$$

If, in equation 18 the angular velocity of the resonance ω_j is known, then eqn. 19 can be rewritten in the form,

$$y = A/x' + \sum_{n=0}^{N} C'_n x'^n . \tag{23}$$

where x' now equals $(w_i - w_j)$. Dropping the primes, the equivalent of eqn. 21 is,

$$yx = \sum_{n=0}^{N+1} D_n x^n , \tag{24}$$

In matrix form, the set of equations become,

$$\mathbf{M}\boldsymbol{D} = \boldsymbol{F} . \tag{25}$$

where $\mathbf{M}$ is a matrix and $\boldsymbol{D}$ and $\boldsymbol{F}$ are vectors,

$$\begin{aligned} M_{m,n} &= x_m^n , \\ F_m &= y_m x_m . \end{aligned}$$

$\mathbf{M}$ is a Vandermonde matrix. Turner (1966) shows that its inverse, $\mathbf{M}^{-1}$, contains terms which are simple function of the variables x_m. The solution is then given by,

$$\boldsymbol{D} = \mathbf{M}^{-1}\boldsymbol{F} . \tag{26}$$

The residue of the pole in eqn. 23 is given by D_0. In the case of four unknowns, if the x_is have the values $\pm\delta$ and $\pm i\delta$, where δ is non-zero, then the residue is just the mean value of the elements of $\boldsymbol{F}$.

Acknowledgements. I wish to thank the editors of the CSIRO journal "Marine and Freshwater Research" for permission to reuse figures from Webb (1981).

References

Anon: Admiralty Tide Tables, Hydrographer of the Navy, London, 1971.

Arbic, B., Karsten, R., and Garrett, C.: On Tidal Resonance in the Global Ocean and the Back-Effect of Coastal Tides upon Open-Ocean Tides, Atmosphere-Ocean, 47, 239–266, 2009.

Easton, A.: The tides of the continent of Australia, Report 37, Horace Lamb Centre for Oceanographic Research, Flinders University of South Australia, 1970.

Egbert, G. and Ray, R.: Estimates of M_2 tidal energy dissipation from TOPEX/Poseidon altimeter data, Journal of Geophysical Research, 106, 22 475–22 502, 2001.

Egbert, G. and Ray, R.: Semi-diurnal and diurnal tidal dissipation from TOPEX/Poseidon altimeter data, Geophysical Research Letters, 30, doi:10.1029/2003GL017 676, 2003.

Garrett, C. and Munk, W.: The age of the Tide and the 'Q' of the Ocean, Deep-Sea Research, 18, 493–504, 1971.

Green, J. A. M.: Ocean tides and resonances, Ocean Dynamics, 60, 1243–1253, 2009.

Grignon, L.: Tidal resonances on the North-West European Shelf, Master's thesis, University of Southampton, School of Ocean and Earth Science, 2005.

Longuet-Higgins, M.: The Eigenfunctions of Laplace's Tidal Equations over a Sphere, Philosophical Transactions of the Royal Society, A262, 511–607, 1968.

Longuet-Higgins, M. and Pond, G. S.: The Free Oscillations of Fluid on a Hemisphere Bounded by Meridians of Longitude, Philosophical Transactions of the Royal Society, A266, 193–223, 1980.

Miller, G. R.: The flux of tidal energy out of the deep ocean, Journal of Geophysical Research, 71, 2485–2489, 1966.

Munk, W. and Cartwright, D.: Tidal Spectroscopy and Prediction, Philosophical Transactions of the Royal Society, A259, 533–581, 1966.

Platzman, G. W., Curtis, G. A., Hansen, K. S., and Slater, R. D.: Normal Modes of the World Ocean. Part II: Description of Modes in the Period Range 8 to 80 Hours, Journal of Physical Oceanography, 11, 579–603, 1981.

Turner, L. R.: Inverse of the Vandermonde Matrix with Applications, NASA Technical Note D-3547, US National Aeronautics and Space Administration, 1966.

Webb, D.: On the Age of the Semi-diurnal Tide, Deep-Sea Research, 20, 847–852, 1973a.

Webb, D.: Tidal Resonance in the Coral Sea, Nature, 243, 511, 1973b.

Webb, D.: A Model of Continental Shelf Resonances, Deep-Sea Research, 23, 1–15, 1976.

Webb, D.: Numerical Model of the Tides in the Gulf of Carpentaria and Arafura Sea, Australian Journal of Marine and Freshwater Research, 32, 31–44, 1981.

Webb, D.: Notes on a 1-D Model of Continental Shelf Resonances, Research and Consultancy Report 85, National Oceanography Centre, Southampton, 2011.